Electron-electron-photon polarization correlations in high-energy bremsstrahlung

D. H. Jakubassa-Amundsen*
Mathematics Institute, University of Munich, 80333 Munich, Germany

(Received 22 October 2018; revised manuscript received 22 November 2018; published 28 December 2018)

A formal derivation of the polarization correlations between the incident electron, the scattered electron, and the emitted bremsstrahlung photon is given. For the sake of demonstration, spin asymmetries pertaining to polarized scattered electrons are determined within the relativistic partial-wave theory. In addition to the sum rule for the polarization correlations relating to an unobserved spin of the scattered electron, three further sum rules are established in coplanar geometry.

DOI: 10.1103/PhysRevA.98.062715

I. INTRODUCTION

Polarization phenomena during the interplay of fast electrons and photons in strong external fields are of widespread interest. Polarization transfer from polarized electrons to photons can be applied for the diagnostics and stability check of spin-polarized electron beams [1,2]. Polarized electron bremsstrahlung serves also as a source of radiation to induce nuclear transitions of specific multipolarities and parities [3]. Moreover, bremsstrahlung from polarized electrons in the mega-electron-volt region or beyond, emitted in a conversion target, may be used as a source for polarized positrons via pair creation [4]. Furthermore, observed polarized photons from electrons of extraterrestric origin may carry information on their sources, for example, on the direction of the magnetic field vector in strongly magnetized media [5].

The most detailed information is provided from a complete experiment on bremsstrahlung, where the polarization state of each of the involved particles has to be specified, in addition to measuring their momentum distribution. Thereby it is assumed that the target has spin zero and remains inert during the collision. Up to now, at most the spin polarization of the incoming electron combined with the polarization of the emitted photon was recorded, while the spin polarization of the scattered electron has remained unobserved [1,2,6–10].

There exist a few theoretical investigations which consider the polarization of both outgoing particles. Using Sommerfeld-Maue scattering states where the spin part of the electronic wave function involves simply a plane-wave spinor, such triple polarization correlations were already studied by Olsen and Maximon [11]. However, calculations were restricted to angle-integrated cross sections at ultrahigh beam energies. Haug [12] formulated the Sommerfeld-Maue theory for arbitrary collision energies and polarizations, but he did not provide numerical results for spin-polarized scattered electrons. For heavy atoms and moderate impact energies, the relativistic partial-wave theory (see, e.g., Refs. [13–15]) has to be applied, where the spin dependence of the electronic scattering states is much more involved. Polarization correlations between beam electrons and bremsstrahlung photons for the triply differential cross section were considered in Refs. [16,17] within this theory, again disregarding the spin polarization of the scattered electrons.

In the present work we provide a general representation of all polarization correlations by making use of the linearity of the scattering states in the respective polarization spinors. The advantage of such a formulation in terms of abstract transition matrix elements is the discovery of sum rules which are obeyed by the polarization correlations. This was demonstrated by Pratt and coworkers in the simpler case of photoionization [18,19], where it was possible to establish a general sum rule [20]. This sum rule could be translated to the doubly differential bremsstrahlung cross section, provided the scattered electron was described by a single pair of partial waves [20]. For the triply differential cross section, but still for unpolarized scattered electrons, it was later proven that this sum rule holds in coplanar geometry without any restriction of the final electronic state [21]. When the spin polarization of the scattered electron is additionally taken into account, we prove the existence of three further sum rules for the polarization correlations. Moreover, we provide numerical results for the polarization transfer from the incoming electron to the scattered electron, which had not been investigated previously.

The paper is organized as follows. Section II provides the formal derivation of the polarization correlations, which are given explicitly in the case of coplanar geometry. Numerical examples within the partial-wave theory, also for noncoplanar geometry, are discussed in Sec. III. The sum rules are established in Sec. IV. A short conclusion follows (Sec. V). Atomic units ($\hbar = m = e = 1$) are used unless indicated otherwise.

II. THEORY

We characterize the incoming electron by the momentum $\boldsymbol{k}_i$, the total energy E_i, and the spin polarization vector $\boldsymbol{\zeta}_i$. Correspondingly, for the scattered electron we use $\boldsymbol{k}_f$, E_f, and $\boldsymbol{\zeta}_f$. The emitted photon is described by its momentum $\boldsymbol{k}$, the frequency $\omega = ck$, and the polarization vector $\boldsymbol{\epsilon}_\lambda$. Our analysis is based on the fact that the electronic scattering states $\psi_i(\boldsymbol{\zeta}_i, \boldsymbol{r})$ and $\psi_f(\boldsymbol{\zeta}_f, \boldsymbol{r})$ are linear in the polarization spinors

*dj@math.lmu.de

$w_i = \sum_{m_i} a_{m_i} \chi_{m_i}$ and $w_f = \sum_{m_s} b_{m_s} \chi_{m_s}$, respectively, where $\chi_{\frac{1}{2}} = \binom{1}{0}$ and $\chi_{-\frac{1}{2}} = \binom{0}{1}$ are the spinor basis vectors [22]. The relations between the coordinates of $\boldsymbol{\zeta}_i = (\zeta_{ix}, \zeta_{iy}, \zeta_{iz}) = (\sin\alpha_s \cos\varphi_s, \sin\alpha_s \sin\varphi_s, \cos\alpha_s)$ and the coefficients a_{m_i} are given by [14,22,23]

$$a_{\frac{1}{2}} = \cos\frac{\alpha_s}{2}\, e^{-i\varphi_s/2}, \quad a_{-\frac{1}{2}} = \sin\frac{\alpha_s}{2}\, e^{i\varphi_s/2}. \tag{2.1}$$

Similar relations hold for the final spin polarization.

Also the photon operator is linear in the polarization vector. It is convenient to expand $\boldsymbol{\epsilon}_\lambda$ in the basis of the circular polarization vectors $\boldsymbol{\epsilon}_\pm$, where $(+)$ and $(-)$ denote, respectively, right-handed and left-handed photons,

$$\boldsymbol{\epsilon}_\lambda^* = \sum_{\sigma=\pm} f_\sigma \boldsymbol{\epsilon}_\sigma^*. \tag{2.2}$$

Using a coordinate system where the z-axis $\boldsymbol{e}_z$ is taken along $\boldsymbol{k}_i$, $\boldsymbol{e}_y$ is taken along $\boldsymbol{k}_i \times \boldsymbol{k}$, and $\boldsymbol{e}_x = \boldsymbol{e}_y \times \hat{\boldsymbol{k}}_i$, the photon momentum $\boldsymbol{k} = k(\sin\theta_k, 0, \cos\theta_k)$ lies in the (x,z) plane (the reaction plane). Accordingly, the circularly polarized photons are characterized by $\boldsymbol{\epsilon}_\pm = (-\cos\theta_k, \mp i, \sin\theta_k)/\sqrt{2}$, fulfilling the orthogonality requirement with respect to $\boldsymbol{k}$.

The linearity in all polarization degrees of freedom allows the triply differential cross section for scattering the electron into the solid angle $d\Omega_f$ while simultaneously emitting a photon into the solid angle $d\Omega_k$ [14,16,17] to be expressed in terms of a triple sum [21]:

$$\begin{aligned}
&\frac{d^3\sigma}{d\omega d\Omega_k d\Omega_f}(\boldsymbol{\zeta}_i, \boldsymbol{\zeta}_f, \boldsymbol{\epsilon}_\lambda^*) = N_0\, |W_{\rm rad}(\boldsymbol{\zeta}_f, \boldsymbol{\zeta}_i)|^2,\\
&W_{\rm rad}(\boldsymbol{\zeta}_f, \boldsymbol{\zeta}_i) = \langle \psi_f(\boldsymbol{\zeta}_f, \boldsymbol{r})|\, \boldsymbol{\alpha}\boldsymbol{\epsilon}_\lambda^* e^{-i\boldsymbol{k}\boldsymbol{r}}\, |\psi_i(\boldsymbol{\zeta}_i, \boldsymbol{r})\rangle\\
&\quad = \sum_{m_i=\pm\frac{1}{2}} a_{m_i} \sum_{m_s=\pm\frac{1}{2}} b_{m_s}^* \sum_{\sigma=\pm} f_\sigma M_{fi}(\boldsymbol{\epsilon}_\sigma^*, m_i, m_s).
\end{aligned} \tag{2.3}$$

The normalization constant is given by $N_0 = \frac{4\pi^2\omega k_f E_i E_f}{c^5 k_i f_{\rm re}}$, where $f_{\rm re}$ is a recoil factor which is negligibly small in our region of interest [24]. $\boldsymbol{\alpha}$ is a vector of Dirac matrices. By means of a partial-wave expansion of the Dirac scattering states ψ_i and ψ_f and of the photon operator $e^{-i\boldsymbol{k}\boldsymbol{r}}$, the matrix elements M_{fi} are readily reduced to a multiple sum over the angular momentum quantum numbers [13]. The one-dimensional radial integrals occurring in these sums can be calculated with the help of the complex-plane rotation method [15,25]. For the formal derivation of the polarization correlations the explicit form of M_{fi} is, however, not needed.

The eight different matrix elements entering into Eq. (2.3) are abbreviated in the following way:

$$\begin{aligned}
M_{fi}\big(\boldsymbol{\epsilon}_\pm^*, \tfrac{1}{2}, \tfrac{1}{2}\big) &= J_\pm, \quad M_{fi}\big(\boldsymbol{\epsilon}_\pm^*, -\tfrac{1}{2}, \tfrac{1}{2}\big) = S_\pm,\\
M_{fi}\big(\boldsymbol{\epsilon}_\pm^*, \tfrac{1}{2}, -\tfrac{1}{2}\big) &= K_\pm, \quad M_{fi}\big(\boldsymbol{\epsilon}_\pm^*, -\tfrac{1}{2}, -\tfrac{1}{2}\big) = T_\pm.
\end{aligned} \tag{2.4}$$

In coplanar geometry, where $\boldsymbol{k}_f$ lies in the reaction plane, there is a symmetry relation for the M_{fi}, based on time-reversal invariance [21],

$$M_{fi}(\boldsymbol{\epsilon}_-^*, -m_i, -m_s) = (-1)^{m_i - m_s}\, M_{fi}(\boldsymbol{\epsilon}_+^*, m_i, m_s), \tag{2.5}$$

which reduces the eight matrix elements to four, since in that case $K_\pm = -S_\mp$ and $T_\pm = J_\mp$. A similar reduction has been established in the theory of photoionization [19].

It follows from the representation (2.3) that the cross section is bilinear in any of the coefficients a_{m_i}, $b_{m_s}^*$, and f_σ. In turn, this leads to a linear dependence on the coordinates of the electron spin vectors, since eliminating the spherical angles α_s and φ_s from Eq. (2.1) one obtains

$$\begin{aligned}
|a_{\pm\frac{1}{2}}|^2 &= \tfrac{1}{2}\,(1 \pm \zeta_{iz}), \quad a_{\frac{1}{2}}^*\, a_{-\frac{1}{2}} = \tfrac{1}{2}\,(\zeta_{ix} + i\,\zeta_{iy}),\\
|b_{\pm\frac{1}{2}}|^2 &= \tfrac{1}{2}\,(1 \pm \zeta_{fz}), \quad b_{\frac{1}{2}}^* b_{-\frac{1}{2}} = \tfrac{1}{2}\,(\zeta_{fx} + i\,\zeta_{fy}).
\end{aligned} \tag{2.6}$$

Also the photon polarization can be represented by a vector $\boldsymbol{\xi} = (\xi_1, \xi_2, \xi_3)$ which enters linearly into the cross section. Following Tseng and Pratt [14], the photon polarization vector $\boldsymbol{\epsilon}_\lambda$ is expanded in the basis $\boldsymbol{\epsilon}_{\lambda_1} = (0,1,0)$ and $\boldsymbol{\epsilon}_{\lambda_2} = (-\cos\theta_k, 0, \sin\theta_k)$ of *linearly* polarized photons:

$$\begin{aligned}
\boldsymbol{\epsilon}_\lambda &= \sum_{k=1}^{2} \beta_k\, \boldsymbol{\epsilon}_{\lambda_k},\\
\beta_1 &= \sin\varphi_\lambda, \quad \beta_2 = \cos\varphi_\lambda \quad (\boldsymbol{\epsilon}_\lambda \text{ linear}),\\
\beta_1 &= \mp\, i/\sqrt{2}, \quad \beta_2 = 1/\sqrt{2} \quad (\boldsymbol{\epsilon}_\lambda = \boldsymbol{\epsilon}_\pm \text{ circular}),
\end{aligned} \tag{2.7}$$

where $0 \leqslant \varphi_\lambda \leqslant \pi$, and the upper sign in the last line is for a right-handed photon and the lower sign is for a left-handed photon. Then $\boldsymbol{\xi}$ is introduced by means of

$$\boldsymbol{\xi} = (2{\rm Re}\beta_1\beta_2^*,\ 2{\rm Im}\beta_1\beta_2^*,\ |\beta_2|^2 - |\beta_1|^2\,). \tag{2.8}$$

It is easily seen that for the circular polarization $\boldsymbol{\epsilon}_\pm$ one has $\xi_1 = \xi_3 = 0$ and $\xi_2 = \mp 1$, while a linearly polarized photon is represented by $\xi_2 = 0$, $\xi_1 = \sin(2\varphi_\lambda)$, and $\xi_3 = \cos(2\varphi_\lambda)$.

Expanding a linearly polarized photon according to Eq. (2.2), i.e., $\boldsymbol{\epsilon}_\lambda(\varphi_\lambda) = (e^{-i\varphi_\lambda}\boldsymbol{\epsilon}_+^* + e^{i\varphi_\lambda}\boldsymbol{\epsilon}_-^*)/\sqrt{2}$, the expansion coefficients f_σ obey

$$|f_+|^2 = |f_-|^2 = \tfrac{1}{2}, \quad f_+^*\, f_- = \tfrac{1}{2}\,(\xi_3 + i\,\xi_1). \tag{2.9}$$

For circularly polarized photons $\boldsymbol{\epsilon}_\pm^*$, the respective relations are

$$\begin{aligned}
|f_+|^2 = 1 &= \tfrac{1}{2}\,(1+\xi_2), \quad |f_-|^2 = f_+^*\, f_- = 0 \quad \text{for } \boldsymbol{\epsilon}_+^*,\\
|f_-|^2 = 1 &= \tfrac{1}{2}\,(1-\xi_2), \quad |f_+|^2 = f_+^*\, f_- = 0 \quad \text{for } \boldsymbol{\epsilon}_-^*.
\end{aligned} \tag{2.10}$$

Therefore the cross section has the following structure,

$$\begin{aligned}
\frac{d^3\sigma}{d\omega d\Omega_k d\Omega_f}(\boldsymbol{\zeta}_i, \boldsymbol{\zeta}_f, \boldsymbol{\epsilon}_\lambda^*) &= \frac{1}{4}\left(\frac{d^3\sigma}{d\omega d\Omega_k d\Omega_f}\right)_0\\
&\times \left(1 + \sum_{jkl} \tilde{C}_{jkl}\, \zeta_{ij}\zeta_{fl}\xi_k\right),
\end{aligned} \tag{2.11}$$

where $(\frac{d^3\sigma}{d\omega d\Omega_k d\Omega_f})_0 = \frac{1}{2}\sum_{\zeta_i,\zeta_f,\lambda} \frac{d^3\sigma}{d\omega d\Omega_k d\Omega_f}$ is the cross section for unpolarized particles, where it is averaged over the initial polarization states and summed over the final polarization states. The coefficients $\tilde{C}_{jkl}$ are called polarization correlations. The subscripts j and l refer, respectively, to the jth and lth coordinates of $\boldsymbol{\zeta}_i$ and $\boldsymbol{\zeta}_f$ (with $1, 2, 3 = x, y, z$), while the subscript k denotes the respective coordinate of $\boldsymbol{\xi}$. Each index

runs from 0 to 3 (excluding the case $j = k = l = 0$), where the absence of a particular coordinate is marked by a zero. We have introduced a tilde in $\tilde{C}_{jkl}$, because the parameters defined in Eq. (2.11) differ from the C_{jkl} introduced by Tseng [16] by a possible sign, due to the different choice of coordinate system (in the original papers, the z axis is taken along $\boldsymbol{k}$ as in the photoionization studies). In coplanar geometry, the seven nonvanishing parameters for unobserved spin of the scattered electron [16] are interrelated by $\tilde{C}_{jk0} = -C_{jk0}$ for $(jk) =$ (12), (31), (20), and (23), while $\tilde{C}_{jk0} = C_{jk0}$ for $(jk) = (03)$, (32), and (11) [21].

A peculiarity of the coplanar geometry is the fact that out of the total $4^3 - 1 = 63$ coefficients $\tilde{C}_{jkl}$ only 31 are nonzero, and only 16 differ from each other. A straightforward evaluation of Eq. (2.3) provides the representation of the nonvanishing $\tilde{C}_{jkl}$ in terms of the matrix elements $J_\pm$ and $S_\pm$. For the unpolarized cross section one obtains

$$\left(\frac{d^3\sigma}{d\omega d\Omega_k d\Omega_f}\right)_0 = N_0\, D_0,$$
$$D_0 = |J_+|^2 + |J_-|^2 + |S_+|^2 + |S_-|^2. \quad (2.12)$$

The polarization correlations of the form $\tilde{C}_{0kl}$, pertaining to an unobserved initial electron spin, are given by

$$\begin{aligned}
\tilde{C}_{021} &= 2\mathrm{Re}(-J_+S_-^* + J_-S_+^*)/D_0 = \tilde{C}_{213},\\
\tilde{C}_{002} &= 2\mathrm{Im}(J_+S_-^* + J_-S_+^*)/D_0 = \tilde{C}_{230},\\
\tilde{C}_{030} &= 2\mathrm{Re}(J_+J_-^* + S_+S_-^*)/D_0 = \tilde{C}_{202},\\
\tilde{C}_{013} &= 2\mathrm{Im}(J_+J_-^* + S_+S_-^*)/D_0 = \tilde{C}_{221},\\
\tilde{C}_{011} &= 2\mathrm{Im}(J_+^*S_+ + J_-S_-^*)/D_0 = -\tilde{C}_{223},\\
\tilde{C}_{032} &= 2\mathrm{Im}(-J_+^*S_+ + J_-S_-^*)/D_0 = \tilde{C}_{200},\\
\tilde{C}_{023} &= (|J_+|^2 - |J_-|^2 + |S_+|^2 - |S_-|^2)/D_0 = -\tilde{C}_{211},
\end{aligned} \quad (2.13)$$

where we have included those parameters which are pairwise identical to $\tilde{C}_{0kl}$. We also define $\tilde{C}_{000} = 1$, which provides us with the further identity $\tilde{C}_{232} = \tilde{C}_{000}$.

Furthermore, there are the polarization correlations for unobserved photon polarization (i.e., the $\tilde{C}_{j0l}$ not yet accounted for):

$$\begin{aligned}
\tilde{C}_{301} &= -2\mathrm{Re}(J_+S_-^* + J_-S_+^*)/D_0 = -\tilde{C}_{133},\\
\tilde{C}_{101} &= 2\mathrm{Re}(J_+J_-^* - S_+S_-^*)/D_0 = \tilde{C}_{333},\\
\tilde{C}_{103} &= 2\mathrm{Re}(J_+S_+^* + J_-S_-^*)/D_0 = \tilde{C}_{331},\\
\tilde{C}_{303} &= (|J_+|^2 + |J_-|^2 - |S_+|^2 - |S_-|^2)/D_0 = \tilde{C}_{131}.
\end{aligned} \quad (2.14)$$

Finally, we list the remaining $\tilde{C}_{jk0}$ for unobserved polarization of the scattered electron:

$$\begin{aligned}
\tilde{C}_{120} &= 2\mathrm{Re}(J_+S_+^* - J_-S_-^*)/D_0 = -\tilde{C}_{312},\\
\tilde{C}_{310} &= -2\mathrm{Im}(-J_+J_-^* + S_+S_-^*)/D_0 = -\tilde{C}_{122},\\
\tilde{C}_{110} &= 2\mathrm{Im}(J_+S_-^* - J_-S_+^*)/D_0 = \tilde{C}_{322},\\
\tilde{C}_{320} &= (|J_+|^2 - |J_-|^2 - |S_+|^2 + |S_-|^2)/D_0 = \tilde{C}_{112}.
\end{aligned} \quad (2.15)$$

A remarkable consequence of the pairwise identities of the polarization correlations is the physical interpretation of the parameter $\tilde{C}_{230}$, which is not directly accessible to experiment for unobserved polarization of the scattered electron [14,23]. By means of $\tilde{C}_{230} = \tilde{C}_{002}$, it can now be identified with the asymmetry resulting from flipping the spin of the electronic final state (for unpolarized beam electrons and photons).

III. THE NONCOPLANAR GEOMETRY AND NUMERICAL RESULTS

In noncoplanar geometry, none of the 63 polarization correlations vanishes identically, and each of them has a different dependence on the eight matrix elements of Eq. (2.4). The parameter D_0, which determines the cross section for unpolarized particles, has the general form

$$\begin{aligned}
D_0 = \tfrac{1}{2}(&|J_+|^2 + |J_-|^2 + |S_+|^2 + |S_-|^2\\
&+ |K_+|^2 + |K_-|^2 + |T_+|^2 + |T_-|^2).
\end{aligned} \quad (3.1)$$

Concerning the polarization correlations, we start with $\tilde{C}_{003}$ and $\tilde{C}_{002}$. They describe, respectively, the creation of longitudinally and perpendicularly spin-polarized scattered electrons from unpolarized electrons (after emitting unpolarized photons):

$$\begin{aligned}
\tilde{C}_{003} = \tfrac{1}{2}(&|J_+|^2 + |J_-|^2 + |S_+|^2 + |S_-|^2\\
&- |K_+|^2 - |K_-|^2 - |T_+|^2 - |T_-|^2)/D_0,\\
\tilde{C}_{002} = \mathrm{Im}(&J_+^*K_+ + J_-^*K_- + S_+^*T_+ + S_-^*T_-)/D_0.
\end{aligned} \quad (3.2)$$

It is seen that $\tilde{C}_{003}$ vanishes in coplanar geometry, in contrast to $\tilde{C}_{002}$. For the numerical calculations, as well as for the measurements, it is more convenient to represent these parameters in terms of relative cross-section differences,

$$\begin{aligned}
\tilde{C}_{003} &= \frac{d\sigma(\zeta_{fz}) - d\sigma(-\zeta_{fz})}{d\sigma_0},\\
\tilde{C}_{002} &= \frac{d\sigma(\zeta_{fy}) - d\sigma(-\zeta_{fy})}{d\sigma_0},
\end{aligned} \quad (3.3)$$

where we have abbreviated

$$\begin{aligned}
d\sigma(\zeta_{fl}) &= \frac{1}{2}\sum_{\zeta_i,\lambda}\frac{d^3\sigma}{d\omega d\Omega_k d\Omega_f}(\boldsymbol{\zeta}_i, \zeta_{fl}\boldsymbol{e}_l, \boldsymbol{\epsilon}_\lambda^*),\\
d\sigma_0 &= d\sigma(\zeta_{fl}) + d\sigma(-\zeta_{fl}),
\end{aligned} \quad (3.4)$$

with $l = z$ or $l = y$. $d\sigma_0$ is the unpolarized cross section defined below Eq. (2.11), and $\boldsymbol{\zeta}_f = \zeta_{fl}\boldsymbol{e}_l$ is characterized by the spherical angles $(\alpha_s, \varphi_s) = (0, 0)$ for $l = z$ and $(\frac{\pi}{2}, \frac{\pi}{2})$ for $l = y$.

The numerical calculations were performed for a ^{208}Pb target within the relativistic partial-wave theory as described in detail in Ref. [24]. The Fortran code RADIAL by Salvat *et al.* [26] was used to obtain the scattering states upon solving the radial Dirac equation. For the high collision energies and photon frequencies in the MeV region considered here, the presence of any bound target electrons can be disregarded, except possibly for small electron and photon angles. Focusing on a large scattering angle, we only took the electron-nucleus potential into account, which is derived from the nuclear charge distribution (available in terms of a

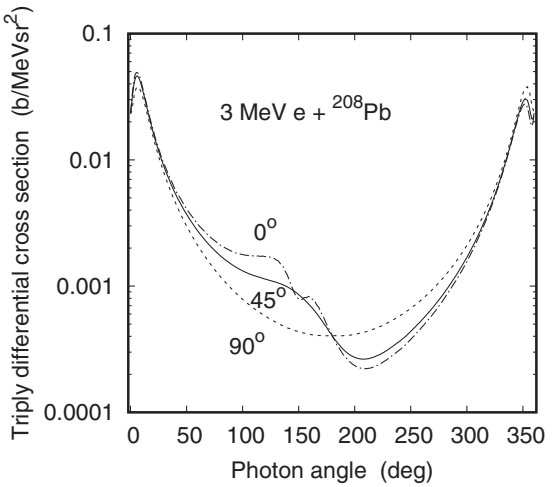

FIG. 1. Triply differential unpolarized bremsstrahlung cross section $(\frac{d^3\sigma}{d\omega d\Omega_k d\Omega_f})_0$ for 3 MeV electrons colliding with ^{208}Pb at the scattering angle $\vartheta_f = 150^\circ$ as a function of photon angle θ_k. The photon frequency is $\omega = 2$ MeV. Shown are results for the azimuthal angles $\varphi_f = 0^\circ$ ($- \cdot - \cdot -$), 45° (————), and 90° ($- - - - -$).

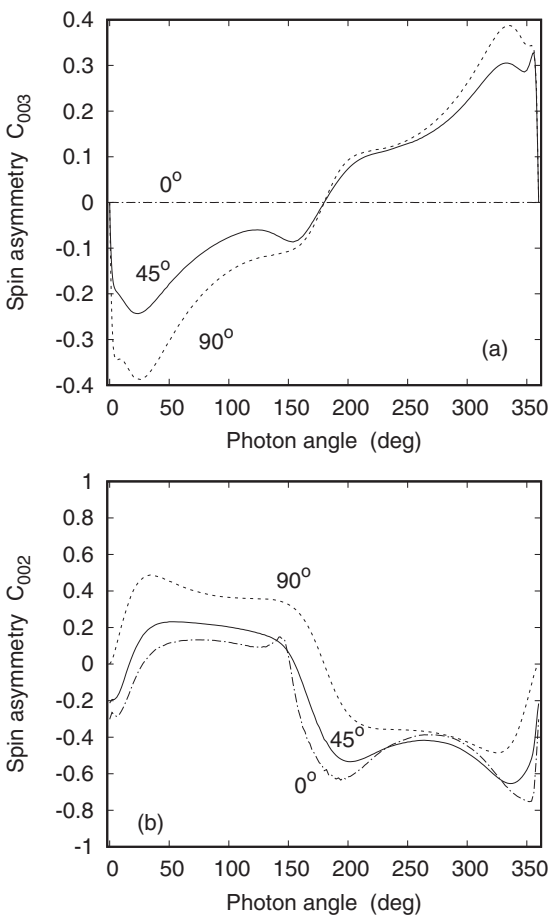

FIG. 2. Polarization correlations (a) $\tilde{C}_{003}$ and (b) $\tilde{C}_{002}$ for 3-MeV electrons colliding with ^{208}Pb and emerging at $\vartheta_f = 150^\circ$ as a function of photon angle θ_k. The photon frequency is 2 MeV. Shown are the results for azimuthal angles $\varphi_f = 0^\circ$ ($- \cdot - \cdot -$), 45° (————), and 90° ($- - - - -$). The wiggles in panel (b) near 180° are due to numerics.

Fourier-Bessel expansion [27]). Satisfactory convergence was obtained by truncating the partial-wave expansions at wave numbers $|\kappa_i| \sim$ 100-120 and $|\kappa_f| \lesssim 25$ for the initial and final states, respectively. The inclusion of too many partial waves (particularly for ψ_f) may lead to numerical instabilities in the backward hemisphere (which show up as wiggles in the θ_k dependence).

The angular dependence of the triply differential cross section for the emission of 2-MeV photons by 3-MeV electrons colliding with lead is shown in Fig. 1. The scattering angle, denoted by ϑ_f, is set to 150° and the azimuthal angle φ_f (between scattered electrons and photons) is fixed at 0°, 45°, and 90°. Angles beyond 180° are covered by the fact that the interval $180^\circ \leqslant \theta_k \leqslant 360^\circ$ at a given φ_f is identical to the interval $180^\circ \geqslant \theta_k \geqslant 0^\circ$ at $\varphi_f + \pi$. In the coplanar case ($\varphi_f = 0$) there is a sharp double-peak structure close to the beam axis and a weaker one in the vicinity of the scattering angle (near 150°). At $\varphi_f = 45^\circ$, this backward double peak has merged into one peak, which at $\varphi_f = 90^\circ$ has completely disappeared, whereas the forward structure persists at all azimuthal angles. Moreover, the photon intensity decreases with φ_f for $\theta_k \lesssim 180^\circ$, but increases at the larger angles. At $\theta_k = 0^\circ$ and 180° the cross section is independent of φ_f, since without the consideration of electron or photon polarizations there is axial symmetry for $\boldsymbol{k}_f$ with respect to the beam axis.

Corresponding to the peak structures in the cross section, there appear extrema in the spin asymmetries near 0° and 150°, the shape of which depends on the electron spin polarization, on the photon frequency, and on the angle φ_f. The spin asymmetries $\tilde{C}_{003}$ and $\tilde{C}_{002}$ are displayed in Fig. 2. It is seen from Fig. 2(a) that, for all azimuthal angles, $\tilde{C}_{003} = 0$ at $\theta_k = 0^\circ = 360^\circ$ and at 180°. The reason is, for $\boldsymbol{k}$ aligned with $\boldsymbol{k}_i$, and also for the (only) observed spin asymmetry $\boldsymbol{\zeta}_f$ aligned with $\boldsymbol{k}_i$, there is axial symmetry for $\boldsymbol{k}_f$ and hence independence of φ_f. This has to be combined with the fact that $\tilde{C}_{003} = 0$ in $\varphi_f = 0$ irrespective of θ_k. There is an increase of the modulus with φ_f in the whole θ_k region, and for $\varphi_f = 90^\circ$, $\tilde{C}_{003}$ is point symmetric with respect to its zero at $\theta_k = 180^\circ$.

The polarization correlation $\tilde{C}_{002}$, shown in Fig. 2(b), remains finite at $\theta_k = 0^\circ$ and 180°, except when $\varphi_f = 90^\circ$. In that particular case (for $\varphi_f = 90^\circ$) the vectors $\boldsymbol{k}_i$, $\boldsymbol{k}$, $\boldsymbol{k}_f$, and $\boldsymbol{\zeta}_f$ are all in the (y, z) plane. This situation corresponds to the one for the parameter $\tilde{C}_{001}$ at $\varphi_f = 0$ [where all these vectors lie in the (x, z) plane], but $\tilde{C}_{001} = \mathrm{Re}(J_+^* K_+ + J_-^* K_- + S_+^* T_+ + S_-^* T_-)/D_0 = 0$ for $\varphi_f = 0$. The spin asymmetry $\tilde{C}_{002}$ is also point symmetric with respect to its zero at 180° in that case. We note that $\tilde{C}_{002}$ can be quite large, up to 80%, for a heavy nucleus like ^{208}Pb. Moreover, $\tilde{C}_{002}$ has a broad shoulder for $30^\circ \lesssim \theta_k \lesssim 150^\circ$ where it increases with φ_f in concord with the decrease of the cross section in that region. Likewise, the maximum in $\tilde{C}_{002}$ near $\theta_k = 150^\circ$ at $\varphi_f = 0$ corresponds to the dip in the respective cross section.

As a second example we have chosen the pair $\tilde{C}_{302}$ and $\tilde{C}_{303}$, which describe, respectively, the spin change and conservation of a longitudinally polarized beam electron (for

unobserved photon polarization). They are given by

$$\tilde{C}_{302} = \mathrm{Im}(J_+^* K_+ + J_-^* K_- - S_+^* T_+ - S_-^* T_-)/D_0,$$
$$\tilde{C}_{303} = \tfrac{1}{2}\,(|J_+|^2 + |J_-|^2 - |S_+|^2 - |S_-|^2 - |K_+|^2 - |K_-|^2 + |T_+|^2 + |T_-|^2)/D_0. \quad (3.5)$$

It follows that $\tilde{C}_{302}$ is vanishing in coplanar geometry, in contrast to $\tilde{C}_{303}$. In order to represent $\tilde{C}_{302}$ in terms of cross-section differences, we first collect all contributions to the cross section which relate to $\boldsymbol{\zeta}_i = \zeta_{iz}\boldsymbol{e}_z$ and $\boldsymbol{\zeta}_f = \zeta_{fy}\boldsymbol{e}_y$, and to unpolarized photons:

$$d\sigma(\zeta_{iz}, \zeta_{fy}) \equiv \sum_\lambda \frac{d^3\sigma}{d\omega d\Omega_k d\Omega_f}(\zeta_{iz}\boldsymbol{e}_z, \zeta_{fy}\boldsymbol{e}_y, \boldsymbol{e}_\lambda^*) = d\sigma_0\ \tfrac{1}{2}(1 + \tilde{C}_{302}\zeta_{iz}\zeta_{fy} + \tilde{C}_{300}\zeta_{iz} + \tilde{C}_{002}\zeta_{fy}). \quad (3.6)$$

Fixing $\zeta_{iz} = 1$, we obtain

$$\frac{d\sigma(1, \zeta_{fy}) - d\sigma(1, -\zeta_{fy})}{d\sigma_0} = \tilde{C}_{302} + \tilde{C}_{002}. \quad (3.7)$$

In a similar way, we obtain $\tilde{C}_{303}$ by replacing the y component of $\boldsymbol{\zeta}_f$ in Eq. (3.7) with the z component:

$$\frac{d\sigma(1, \zeta_{fz}) - d\sigma(1, -\zeta_{fz})}{d\sigma_0} = \tilde{C}_{303} + \tilde{C}_{003}. \quad (3.8)$$

Since it is not possible to isolate $\tilde{C}_{302}$ and $\tilde{C}_{303}$, they are not directly accessible to experiment. Instead, the knowledge of $\tilde{C}_{002}$ and $\tilde{C}_{003}$ from Eq. (3.3) is mandatory in order to provide $\tilde{C}_{302}$ and $\tilde{C}_{303}$. Their angular dependence is depicted in Fig. 3. For longitudinal $\boldsymbol{\zeta}_f$ there is again axial symmetry if $\theta_k = 0^\circ$ or 180°, such that at these two angles, $\tilde{C}_{303}$ is independent of φ_f. $\tilde{C}_{302}$ remains close to 60% in a large regime of photon angles at $\varphi_f = 90^\circ$, decreasing gradually as φ_f tends to zero. In $\tilde{C}_{303}$ the peak near 150° is very sharp for $\varphi_f = 0$, and this spin asymmetry is near 0° close to unity for all three values of φ_f. Note that at $\varphi_f = 45^\circ$, both $\tilde{C}_{303}$ and $\tilde{C}_{302}$ still have a prominent peak near 150°. For $\varphi_f = 90^\circ$, $\tilde{C}_{302}$ and $\tilde{C}_{303}$ are mirror symmetric with respect to the vertical line drawn through 180°. This symmetry property of the polarization correlations investigated here is related to the fact that, in the 90° geometry, all four electron vectors lie in the (y, z) plane. In turn, this plane is perpendicular to the reaction plane where $\boldsymbol{k}$ resides. Therefore (up to a sign in the case of unobserved $\boldsymbol{\zeta}_i$) the spin asymmetry does not change upon reflection of $\boldsymbol{k}$ by the (y, z) plane (i.e., when θ_k is replaced by $2\pi - \theta_k$).

We have also investigated the change of the four selected spin asymmetries with beam energy, photon frequency, and target species. When lowering the nuclear charge, we have found a decrease of the modulus of all the studied polarization correlations except $\tilde{C}_{302}$. Large modifications are predicted when ω is moved to the short-wavelength limit (SWL). This is displayed in Fig. 4(a) for a kinetic energy $E_{i,\mathrm{kin}}$ of 3 MeV and $\omega = 2.9$ MeV at $\varphi = 45^\circ$ where all spin asymmetries are nonvanishing. There is a drastic reduction of $\tilde{C}_{302}$ except at the foremost angles. The peak of $\tilde{C}_{303}$ near 150° has changed into a double-peak structure. Consequently there are now three

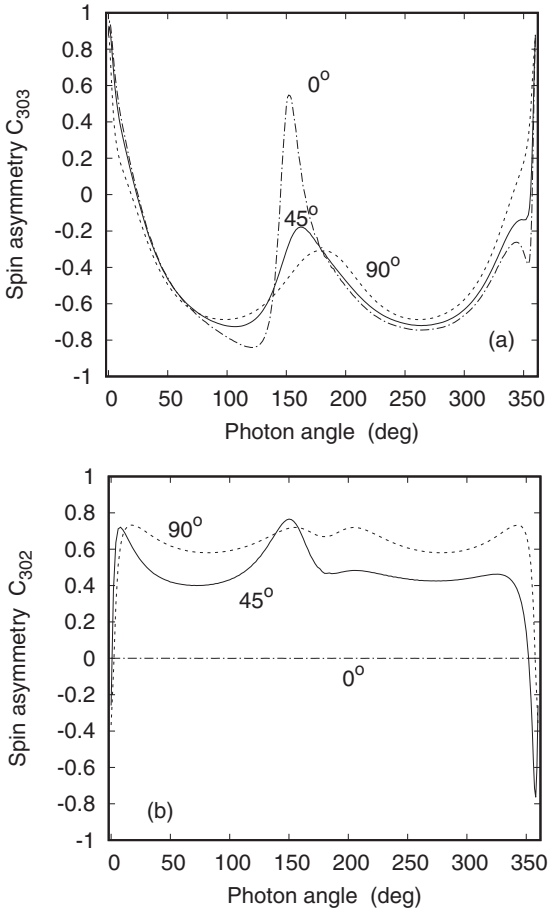

FIG. 3. Same as Fig. 2, but for the polarization correlations (a) $\tilde{C}_{303}$ and (b) $\tilde{C}_{302}$.

angular regions (near 60°, 180°, and 300°) where $|\tilde{C}_{303}|$ is large, up to 80%. Concerning the other two spin asymmetries, the minimum of $\tilde{C}_{003}$ near 150° has turned into a pronounced maximum, such that $\tilde{C}_{003}$ has a negative slope at 180° when ω is close to the SWL. Also $\tilde{C}_{002}$ increases by a factor of 2 in the plateau region $30^\circ \lesssim \theta_k \lesssim 150^\circ$. It should be remarked that the corresponding SWL cross section is an order of magnitude higher close to the beam axis and drops by about a factor of 10^{-4} between $\theta_k \approx 0^\circ$ and 180°.

When the collision energy is increased to 5 MeV (at fixed ratio $\omega/E_{i,\mathrm{kin}} = 2/3$), there are moderate changes in both the magnitude and the shape of all angular distributions. The situation is completely different when the collision energy is lowered to the atomic physics regime, where the screening by the target electrons has to be taken into account. Actually, as shown in Fig. 4(b), at the backward scattering angle of 150°, screening changes the cross section and the polarization correlations mostly by 5% (or less, except in the extrema), even at a rather low collision energy of 0.3 MeV. (For this energy, the expansion was truncated at $|\kappa_i| = 25$ and $|\kappa_f| = 9$.) However, while the intensity increases globally with decreasing $E_{i,\mathrm{kin}}$, there are drastic changes in the angular distribution of the polarization correlations. In particular, for $\tilde{C}_{303}$, the maximum near 160° is turned into a minimum

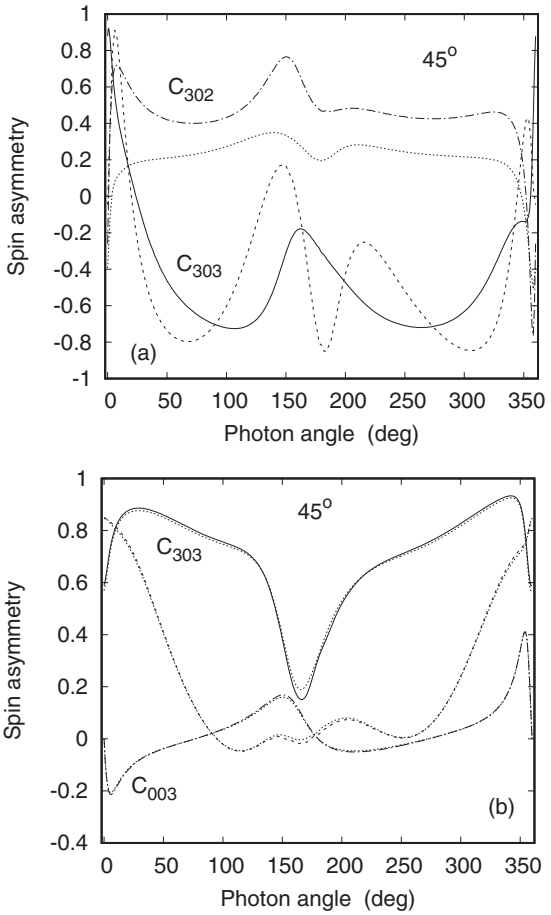

FIG. 4. Polarization correlations for electrons scattering from ^{208}Pb into the angles $\vartheta_f = 150^\circ$ and $\varphi_f = 45^\circ$ as a function of the photon angle. (a) $\tilde{C}_{302}$ and $\tilde{C}_{303}$ for $E_{i,\mathrm{kin}} = 3$ MeV and a photon frequency of $\omega = 2$ MeV ($-\cdot-\cdot-$, $\tilde{C}_{302}$; ———, $\tilde{C}_{303}$) and $\omega = 2.9$ MeV ($\cdots\cdots$, $\tilde{C}_{302}$; $-\,-\,-\,-\,-$, $\tilde{C}_{303}$). (b) $\tilde{C}_{003}$ and $\tilde{C}_{303}$ for the fixed ratio $\omega/E_{i,\mathrm{kin}} = 2/3$. Atomic potential (provided by Haque *et al.* within an optical model prescription [28]): $\tilde{C}_{303}$ (———) and $\tilde{C}_{003}$ ($-\cdot-\cdot-$) at 0.3 MeV; $\tilde{C}_{303}$ ($-\,-\,-\,-\,-$) at 0.9 MeV. Point-nucleus potential: Results are marked by ($\cdots\cdots$) and follow closely the respective curves for the atomic potential.

when the energy is lowered by one order of magnitude (see Fig. 4).

Nuclear size effects are important for heavy nuclei and collision energies beyond the MeV region, if the momentum transfer is high. Already for $E_{i,\mathrm{kin}} = 3$ MeV and $\vartheta_f = 150^\circ$, the cross section is reduced by up to 10% in the backward region ($150^\circ \lesssim \theta_k \lesssim 210^\circ$). The polarization correlations, being cross section ratios, are affected less (well below 5%). At forward angles, the electron–point-nucleus potential is sufficient for accurate results.

IV. SUM RULES IN COPLANAR GEOMETRY

Let us first study the case of unpolarized beam electrons. In this case, the average over $\boldsymbol{\zeta}_i$ eliminates all contributions to the cross section which depend on its coefficients ζ_{ij}, such that the triply differential cross section reduces to

$$\frac{1}{2}\sum_{\zeta_i}\frac{d^3\sigma}{d\omega d\Omega_k d\Omega_f}(\boldsymbol{\zeta}_i,\boldsymbol{\zeta}_f,\boldsymbol{\epsilon}_\lambda^*) = \frac{1}{4}\left(\frac{d^3\sigma}{d\omega d\Omega_k d\Omega_f}\right)_0 \times[1+\tilde{C}_{002}\zeta_{fy}+\tilde{C}_{030}\xi_3+\tilde{C}_{011}\zeta_{fx}\xi_1+\tilde{C}_{013}\zeta_{fz}\xi_1 + \tilde{C}_{021}\zeta_{fx}\xi_2+\tilde{C}_{032}\zeta_{fy}\xi_3+\tilde{C}_{023}\zeta_{fz}\xi_2]. \quad (4.1)$$

The seven polarization correlations entering into Eq. (4.1) obey the following sum rule:

$$C_{023}^2+\left(C_{021}^2+C_{002}^2\right)+\left(C_{030}^2+C_{013}^2\right) + \left(C_{011}^2-C_{032}^2\right)=1. \quad (4.2)$$

Here we have omitted the tilde since $\tilde{C}_{jkl}^2 = C_{jkl}^2$ throughout. The proof of this sum rule is straightforward. It is achieved by multiplying Eq. (4.2) with D_0 from Eq. (2.12) and then considering each term in brackets separately. This is done with the help of the representation (2.13), using the identities $[\mathrm{Re}(z)]^2+[\mathrm{Im}(z)]^2 = |z|^2$, $\mathrm{Re}(z) = \mathrm{Re}(z^*) = \frac{1}{2}(z+z^*)$, and $\mathrm{Im}(z) = -\mathrm{Im}(z^*) = \frac{1}{2i}(z-z^*)$.

If, instead, the polarization of the scattered electron is not observed, only the parameters $\tilde{C}_{jk0}$ are present in the cross section:

$$\sum_{\zeta_f}\frac{d^3\sigma}{d\omega d\Omega_k d\Omega_f}(\boldsymbol{\zeta}_i,\boldsymbol{\zeta}_f,\boldsymbol{\epsilon}_\lambda^*) = \frac{1}{2}\left(\frac{d^3\sigma}{d\omega d\Omega_k d\Omega_f}\right)_0 \times[1+\tilde{C}_{200}\zeta_{iy}+\tilde{C}_{030}\xi_3+\tilde{C}_{110}\zeta_{ix}\xi_1+\tilde{C}_{310}\zeta_{iz}\xi_1 + \tilde{C}_{120}\zeta_{ix}\xi_2+\tilde{C}_{320}\zeta_{iz}\xi_2+\tilde{C}_{230}\zeta_{iy}\xi_3]. \quad (4.3)$$

The termwise correspondence between $\tilde{C}_{jk0}$ of Eq. (4.3) and $\tilde{C}_{0kj}$ in Eq. (4.1) upon the formal substitution $S_+ \mapsto S_-$ and $S_- \mapsto S_+$ leads to a similar sum rule (see also Ref. [21]):

$$C_{320}^2+\left(C_{120}^2+C_{200}^2\right)+\left(C_{030}^2+C_{310}^2\right)+\left(C_{110}^2-C_{230}^2\right)=1. \quad (4.4)$$

The last case to be studied concerns polarized electrons, but unpolarized photons. The corresponding cross section is given by

$$\sum_{\lambda}\frac{d^3\sigma}{d\omega d\Omega_k d\Omega_f}(\boldsymbol{\zeta}_i,\boldsymbol{\zeta}_f,\boldsymbol{\epsilon}_\lambda^*) = \frac{1}{2}\left(\frac{d^3\sigma}{d\omega d\Omega_k d\Omega_f}\right)_0 \times[1+\tilde{C}_{303}\zeta_{iz}\zeta_{fz}+\tilde{C}_{103}\zeta_{ix}\zeta_{fz}+\tilde{C}_{200}\zeta_{iy}+\tilde{C}_{002}\zeta_{fy} + \tilde{C}_{301}\zeta_{iz}\zeta_{fx}+\tilde{C}_{101}\zeta_{ix}\zeta_{fx}+\tilde{C}_{202}\zeta_{iy}\zeta_{fy}]. \quad (4.5)$$

The formal substitution $S_- \mapsto iJ_-$ and $J_- \mapsto -iS_-$ in the parameters appearing in Eq. (4.3) provides the correspondence to the parameters $\tilde{C}_{j0l}$ in Eq. (4.5). This leads to the third sum rule:

$$C_{303}^2+\left(C_{103}^2+C_{200}^2\right)+\left(C_{002}^2+C_{301}^2\right) + \left(C_{101}^2-C_{202}^2\right)=1. \quad (4.6)$$

From Figs. 2(b) and 3(a) it follows that, at θ_k close to zero, this sum rule is already exhausted to about 90% by C_{002} and C_{303} alone.

There exists also a fourth sum rule, involving the squares of all polarization correlations pertaining to unpolarized or

circularly polarized photons. Arranged in increasing order of the indices jkl, one has

$$C^2_{002}+C^2_{021}+C^2_{023}+C^2_{101}+C^2_{103}+C^2_{120}+C^2_{122}+C^2_{200}+C^2_{202}+C^2_{221}+C^2_{223}+C^2_{301}+C^2_{303}+C^2_{320}+C^2_{322}=3. \tag{4.7}$$

From the representation (2.13)–(2.15) of the $\tilde{C}_{jkl}$ appearing in Eq. (4.7), it follows that all of them are different functions of $J_\pm$ and $S_\pm$. Moreover, they represent the maximum set of linearly independent polarization correlations. Equation (4.7) can be proven by expressing those parameters in Eqs. (4.2) and (4.4), which pertain to linearly polarized photons ($k=1$ or $k=3$), in terms of parameters of the form C_{j0l} or C_{j2l} with the help of the pairwise identities provided in Eqs. (2.13)–(2.15). Subsequently, all three sum rules have to be added.

V. CONCLUSION

By using an abstract representation of the bremsstrahlung transition matrix element where only the spin degrees of freedom are treated explicitly, we were able to give a parametrization of the cross section for coincident photon and electron detection in terms of the coordinates of the polarization vectors. This enabled us to establish sum rules for subsets of the polarization correlations if the electron is scattered into the reaction plane. These sum rules are valid irrespective of the theory applied to describe the bremsstrahlung process, provided a first-order treatment of the photon field is sufficient. They can be used to test model-independently the accuracy of the numerical calculations, and they can help to determine spin asymmetries for which an experimental observation is not possible.

We have used the relativistic partial-wave theory to provide estimates for some spin asymmetries pertaining to a fixed polarization of the electronic scattering states, while disregarding any photon polarization. In our examples of a ^{208}Pb target and a ratio of 2/3 (or higher) between photon frequency and beam energy, we predict spin asymmetries amounting up to 40-80% at collision energies of a few MeV.

With the advance of polarized beam techniques and efficient detectors [29,30], coincidence experiments on polarization transfer will be feasible in the near future to challenge the theoretical predictions. The geometry of such $(e,e'\gamma)$ experiments can be chosen in a particular way to maximize the relativistic and magnetic interaction effects. The comparison of accurate measurements with results from state-of-the-art bremsstrahlung calculations may shed light on the possible existence of two-photon processes, like virtual excitation of the target nucleus.

ACKNOWLEDGMENT

I would like to thank A. K. F. Haque for supplying the static potential of atomic lead.

[1] O. Kovtun, V. Tioukine, A. Surzhykov, V. A. Yerokhin, B. Cederwall, and S. Tashenov, Phys. Rev. A **92**, 062707 (2015).
[2] F. Nillius and K. Aulenbacher, PoS **PSPT2015**, 753 (2016).
[3] K. Govaert *et al.*, Nucl. Instrum. Methods Phys. Res., Sect. A **337**, 265 (1994).
[4] J. Dumas, J. Grames, and E. Voutier, AIP Conf. Proc. **1160**, 120 (2009).
[5] F. Lei *et al.*, Space Sci. Rev. **82**, 309 (1997).
[6] E. Haug and W. Nakel, *The Elementary Process of Bremsstrahlung* (World Scientific, Singapore, 2004).
[7] F. Nillius and K. Aulenbacher, J. Phys.: Conf. Ser. **298**, 012024 (2011).
[8] S. Tashenov, T. Bäck, R. Barday, B. Cederwall, J. Enders, A. Khaplanov, Y. Poltoratska, K.-U. Schässburger, and A. Surzhykov, Phys. Rev. Lett. **107**, 173201 (2011).
[9] R. Märtin, G. Weber, R. Barday, Y. Fritzsche, U. Spillmann, W. Chen, R. D. DuBois, J. Enders, M. Hegewald, S. Hess, A. Surzhykov, D. B. Thorn, S. Trotsenko, M. Wagner, D. F. A. Winters, V. A. Yerokhin, and T. Stöhlker, Phys. Rev. Lett. **108**, 264801 (2012).
[10] S. Tashenov, T. Bäck, R. Barday, B. Cederwall, J. Enders, A. Khaplanov, Y. Fritzsche, K. -U. Schässburger, A. Surzhykov, V. A. Yerokhin, and D. H. Jakubassa-Amundsen, Phys. Rev. A **87**, 022707 (2013).
[11] H. Olsen and L. C. Maximon, Phys. Rev. **114**, 887 (1959).
[12] E. Haug, Phys. Rev. **188**, 63 (1969).
[13] H. K. Tseng and R. H. Pratt, Phys. Rev. A **3**, 100 (1971).
[14] H. K. Tseng and R. H. Pratt, Phys. Rev. A **7**, 1502 (1973).
[15] V. A. Yerokhin and A. Surzhykov, Phys. Rev. A **82**, 062702 (2010).
[16] H. K. Tseng, J. Phys. B **35**, 1129 (2002).
[17] R. A. Müller, V. A. Yerokhin, and A. Surzhykov, Phys. Rev. A **90**, 032707 (2014).
[18] R. H. Pratt, R. D. Levee, R. L. Pexton, and W. Aron, Phys. Rev. **134**, A898 (1964).
[19] R. D. Schmickley and R. H. Pratt, Phys. Rev. **164**, 104 (1967).
[20] R. H. Pratt, R. A. Müller, and A. Surzhykov, Phys. Rev. A **93**, 053421 (2016).
[21] D. H. Jakubassa-Amundsen, Eur. Phys. J. D **71**, 209 (2017).
[22] M. E. Rose, *Relativistic Electron Theory* (Wiley, New York, 1961).
[23] D. H. Jakubassa-Amundsen, Phys. Rev. A **82**, 042714 (2010).
[24] D. H. Jakubassa-Amundsen, Phys. Rev. A **93**, 052716 (2016).
[25] C. M. Vincent and H. T. Fortune, Phys. Rev. C **2**, 782 (1970).
[26] F. Salvat, J. M. Fernández-Varea, and W. Williamson, Jr., Comput. Phys. Commun. **90**, 151 (1995).
[27] H. De Vries, C. W. De Jager, and C. De Vries, At. Data Nucl. Data Tables **36**, 495 (1987).
[28] A. K. F. Haque, M. A. Uddin, D. H. Jakubassa-Amundsen, and B. C. Saha, J. Phys. B **51**, 175202 (2018).
[29] R. Barday *et al.*, J. Phys.: Conf. Ser. **298**, 012022 (2011).
[30] S. Tashenov, Nucl. Instrum. Methods Phys. Res., Sect. A **640**, 164 (2011).